4 RESULTS

4.1 Chemical Composition

The chemical compositions of the experimental grain refiners are given in Table 4.1, which shows that grain refiners with a wide range of Ti and B contents were studied.

Table 4.1: Chemical compositions of experimental and commercial grain refiners

Element	Elec1A	Elec1B	Ind1A	Ind2A	Ind1B	Ind2B	Arc2B	KBM AlTiB
Al	Balance	Balance	Balance	Balance	Balance	Balance	Balance	Balance
Cu	0.002	0.001	0.003	0.001	0.001	0.001	0.01	0.001
Mg	0.005	0.003	0.015	0.015	0.008	0.002	0.01	0.002
Si	0.15	0.16	0.40	0.42	0.21	0.24	0.25	0.11
Fe	0.25	0.22	0.29	0.28	0.23	0.21	0.17	0.17
Mn	0.06	0.07	0.10	0.06	0.09	0.06	0.07	0.001
Ni	0.012	0.013	0.10	0.03	0.012	0.016	0.01	0.009
Zn	0.04	0.05	0.17	0.005	0.11	0.05	0.01	0.018
Ti	2.40	1.91	2.64	3.13	6.40	3.41	6.98	4.87
Pb	0.001	0.001	0.001	0.001	0.001	0.001	0.01	0.001
B	0.57	0.31	0.43	0.41	1.04	0.49	1.01	1.03

The titanium-to-boron ratio for each grain refiner was calculated from values in Table 4.1 and is given in Table 4.2. In all grain refiners the titanium-to-boron ratio is far higher than the stoichiometric requirement for the formation of TiB_2, which is 2.22.

Table 4.2: Titanium-to-boron ratio of different alloys

Elements	Wt%							
	Elec1A	**Elec1B**	**Ind1B**	**Ind2B**	**Ind1A**	**Ind2A**	**Arc2B**	**KBM**
Ti	2.40	1.91	6.40	3.41	2.64	3.13	6.98	4.87
B	0.57	0.31	1.04	0.49	0.43	0.41	1.01	1.03
Ti: B	4.20	6.20	6.20	7.00	6.10	7.60	6.90	4.70

4.2 Microstructural Examination

The experimental grain refiners were observed with optical and scanning electron microscopes and showed an aluminium matrix, needle-like grey phases identified by EDS as

$TiAl_3$, prismatic particles of brighter phase, embedded both in the matrix and the $TiAl_3$ identified by EDS as TiB_2. The matrix showed also the presence of silicon.

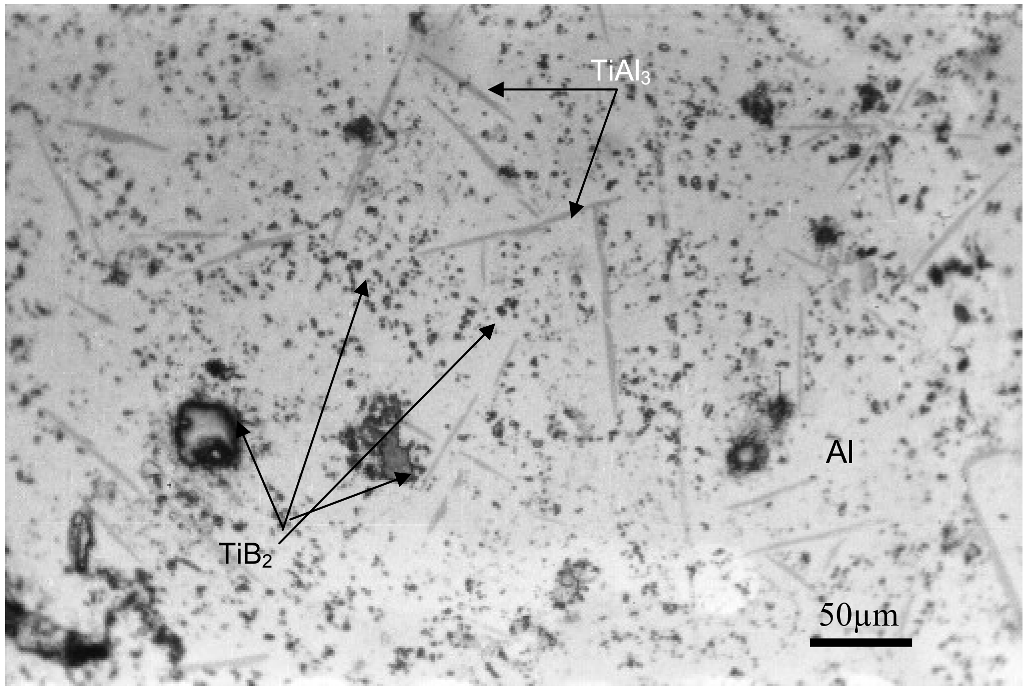

Figure 4.1 Typical microstructure of alloy Elec1A

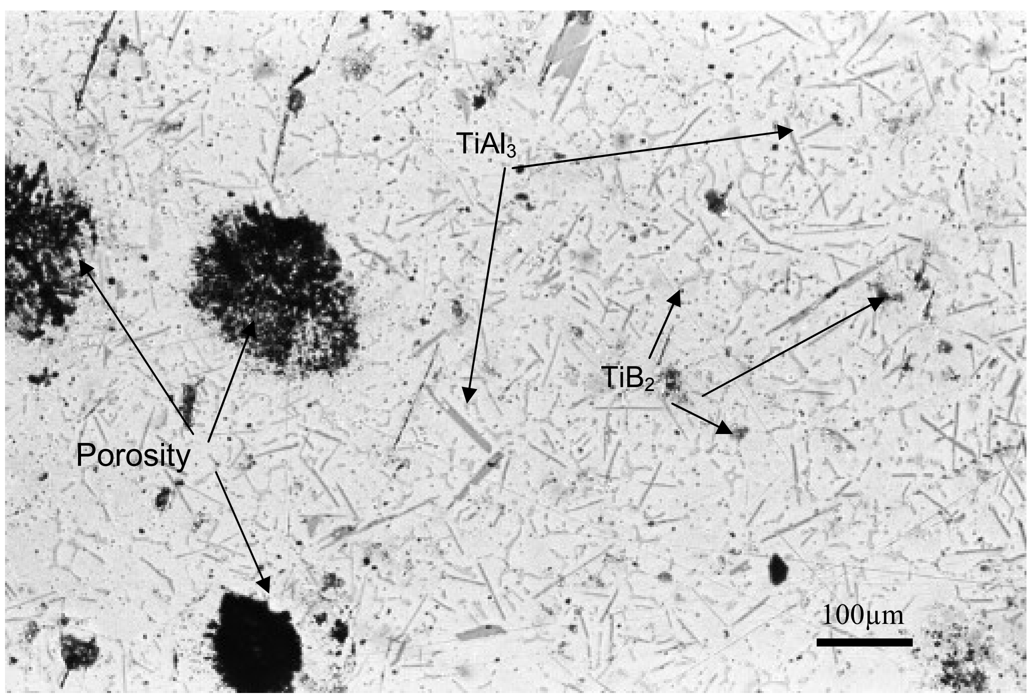

Figure 4.2: Typical microstructure of alloy Ind1A

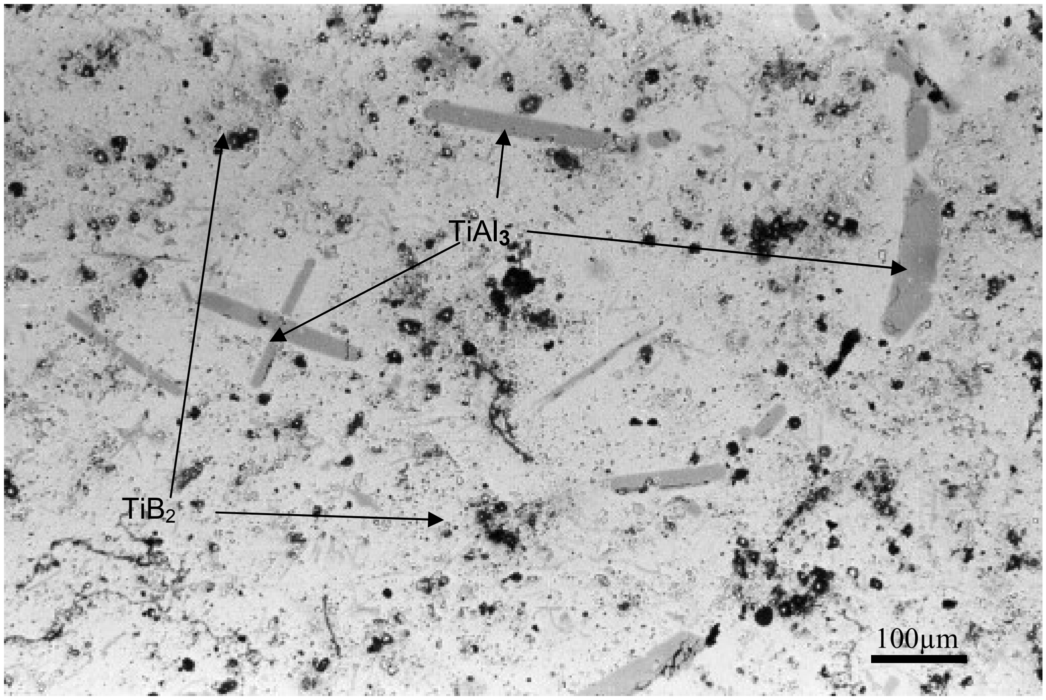

Figure 4.3: Typical microstructure of alloy Ind1B

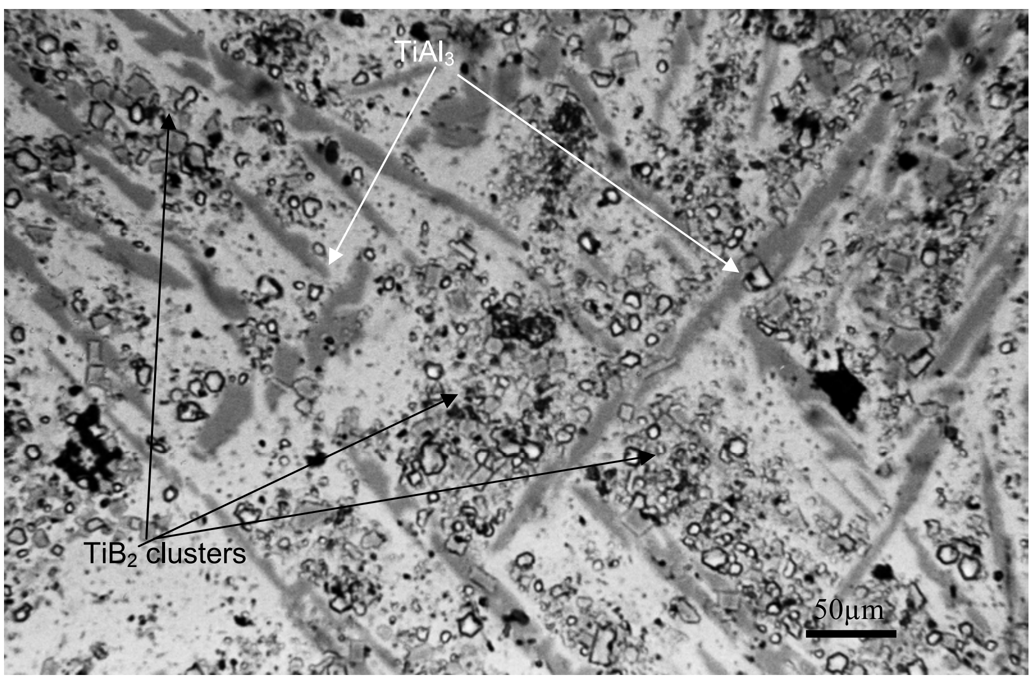

Figure 4.4: Typical microstructure of alloy Arc2B

The size of $TiAl_3$ particles varied and the thinnest were found in alloys of low titanium content, that is, Elec1A, Elec1B, Ind1A and Ind2B. In alloys with high titanium content like Ind1B and

Arc2B, the $TiAl_3$ particles were very thick. In the case of Arc2B, the needle-like particles were zebra-striped in a kind of network as can be seen from Figure 4.4. Appendix A illustrates the increase of TiA_3 thickness with increasing titanium content. The dispersion and the size of the TiB_2 particles varied as well. These particles appeared to be dispersed throughout the aluminium matrix in alloys of high titanium and boron contents (Figure 4.3 and Figure 4.4). In alloys with low Ti and B contents, the $TiAl_3$ particles were very thin with associated clusters of TiB_2 particles. $TiAl_3$ particles sometimes appeared in star formation, particularly in alloy Elec1B. Such a microstructure is shown in Figures 4.5. Figure 4.6 shows large titanium aluminide particles in a random dispersion of TiB_2 particles in alloy Ind1B. This microstructure shows how large the $TiAl_3$ particles could appear in grain refiners of high titanium content.

In all cases, TiB_2 particles showed prismatic and hexagonal morphologies as shown in Figure 4.7. Some of them showed fractures possibly as a result of metallographic preparation. This difference in morphology was characteristic of all grain refiners regardless of the titanium and boron contents. Figure 4.8 shows a facetted TiB_2 particle with an almost perfect hexagonal shape. The appearance of these particles in the plane of the section depends of course on the orientation of the section. Spectra of the phases in the grain refiners are shown in Appendix B.

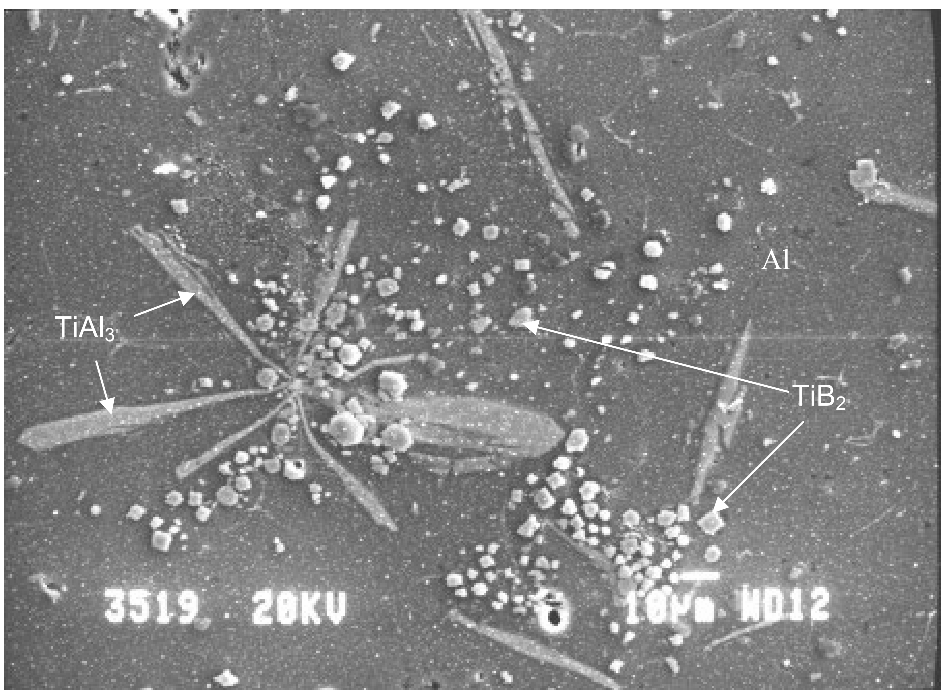

Figure 4.5: $TiAl_3$ in star-like formation and TiB_2 particles in alloy Elec1B

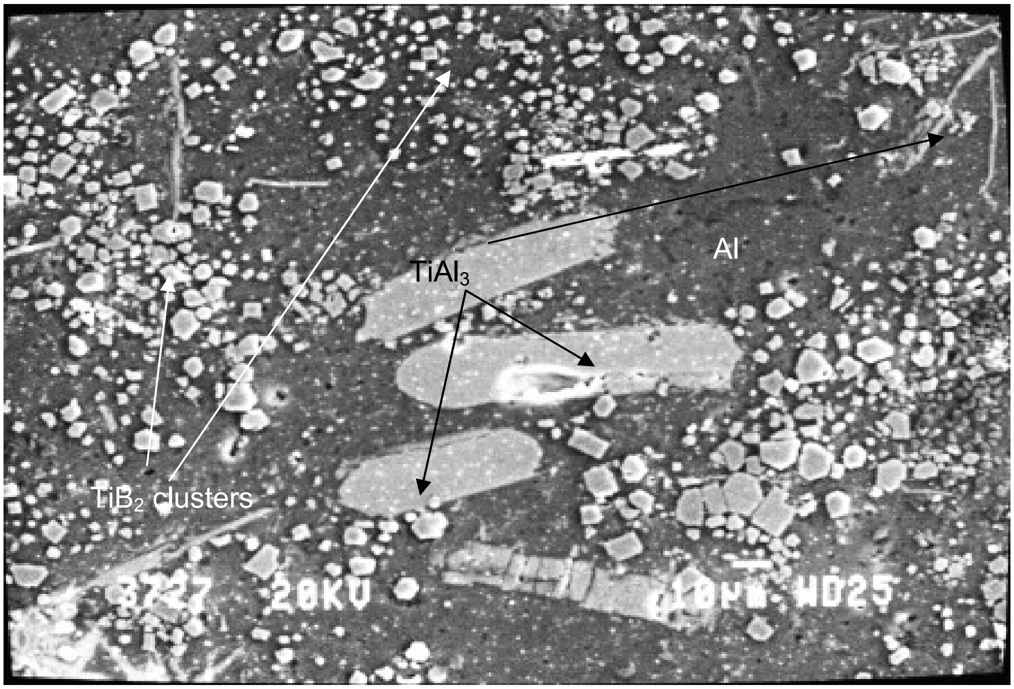

Figure 4 6: Large $TiAl_3$ particles and TiB_2 particles in alloy Ind1B

.

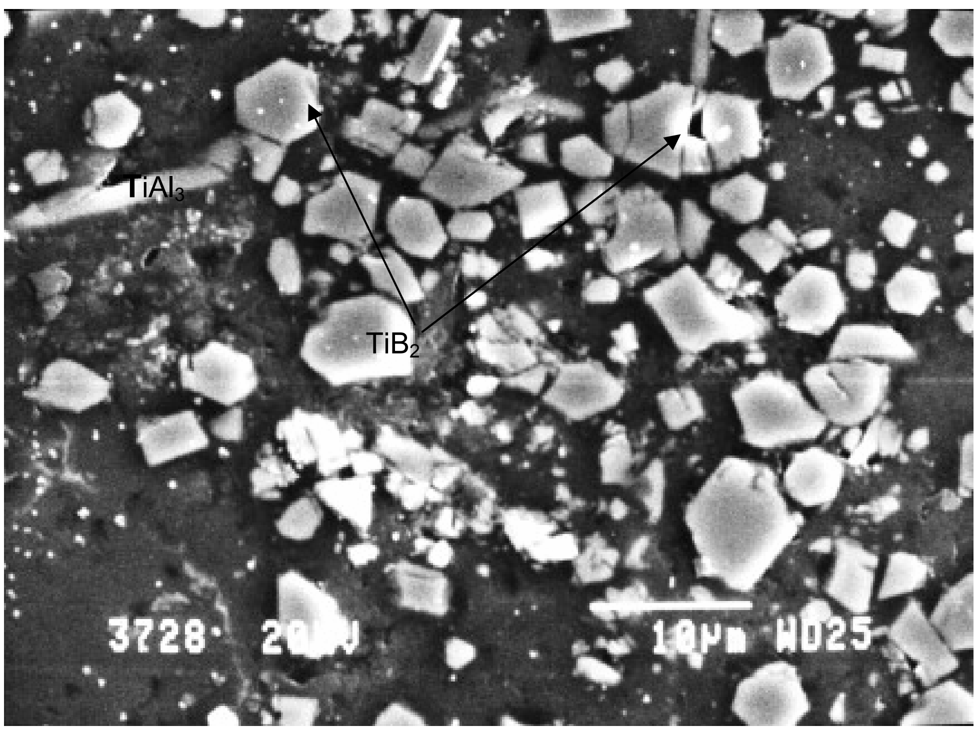

Figure 4.7: $TiAl_3$ and TiB_2 particles in alloy Ind1B

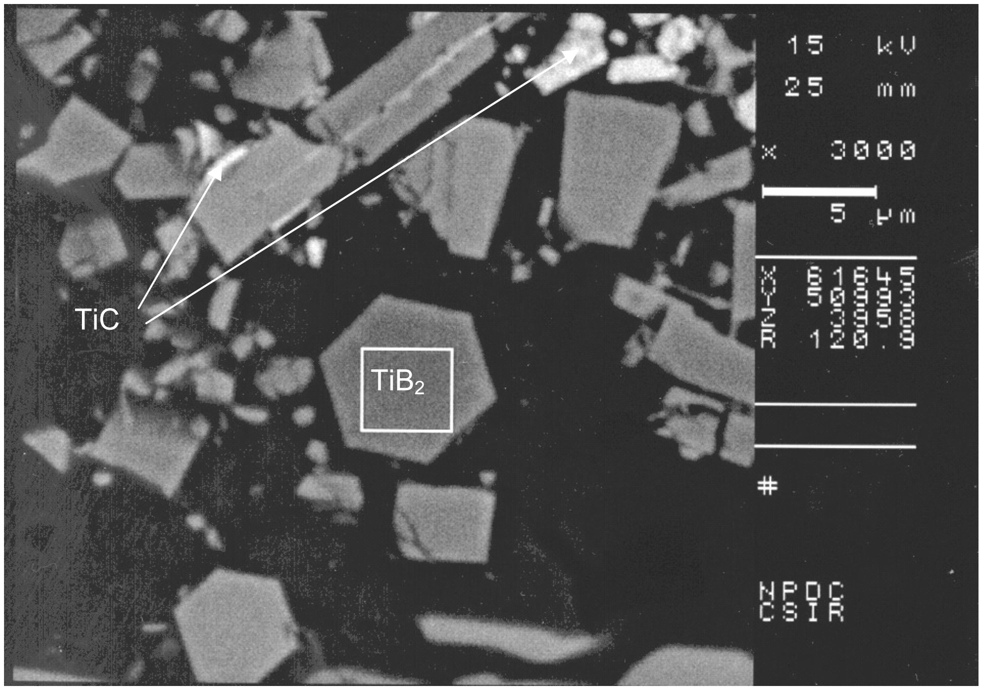

Figure 4.8: Idiomorphic TiB_2 particles in alloy Arc2B

Alloys Arc2B in Figure 4.9 and Ind2B in Figure 4.10 also showed white particles identified by EDS as titanium carbide (TiC). From these figures, it appears that the TiC particles were agglomerated in enormous and compacted particles as big as 20μm in size. TiC particles in the experimental grain refiners were coarser than in commercial Al-Ti-C grain refiners.

By etching the samples with modified Keller's reagent, it was possible to highlight the grain boundaries and to obtain contrast between the different precipitate particles. Thus TiB_2 particles could be distinguished from the other particles in the aluminium matrix. It was also possible to determine the position of the different particles within the grains. The $TiAl_3$ and TiB_2 phases appeared as white particles with the morphologies described earlier. Another phase, also prismatic appeared as grey particles in the matrix. EDS identified the grey phase as silicon. Silicon mostly appeared at the grain boundaries indicating silicon below 1.6%. Figure 4.11 illustrates such a microstructure for alloy Ind2B. TiB_2 particles appeared in the aluminium matrix with no preference for the grain boundaries. Entire clusters of TiB_2 particles were found within grain boundaries. Silicon particles appeared mostly at the grain boundaries. Some isolated particles could also be seen outside the grain boundaries.

Examination of powders obtained after electrolytic dissolution of the matrix showed $TiAl_3$ and TiB_2 particles (Figure 4.12). Carbide particles were not observed, probably due to their low concentration.

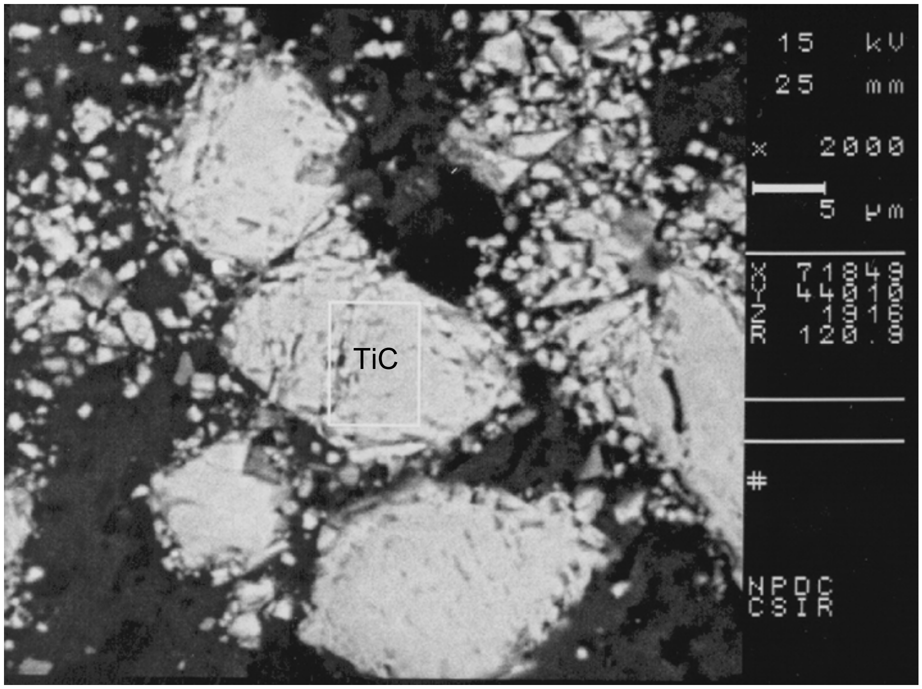

Figure 4.9: TiC particles in alloy Arc2B

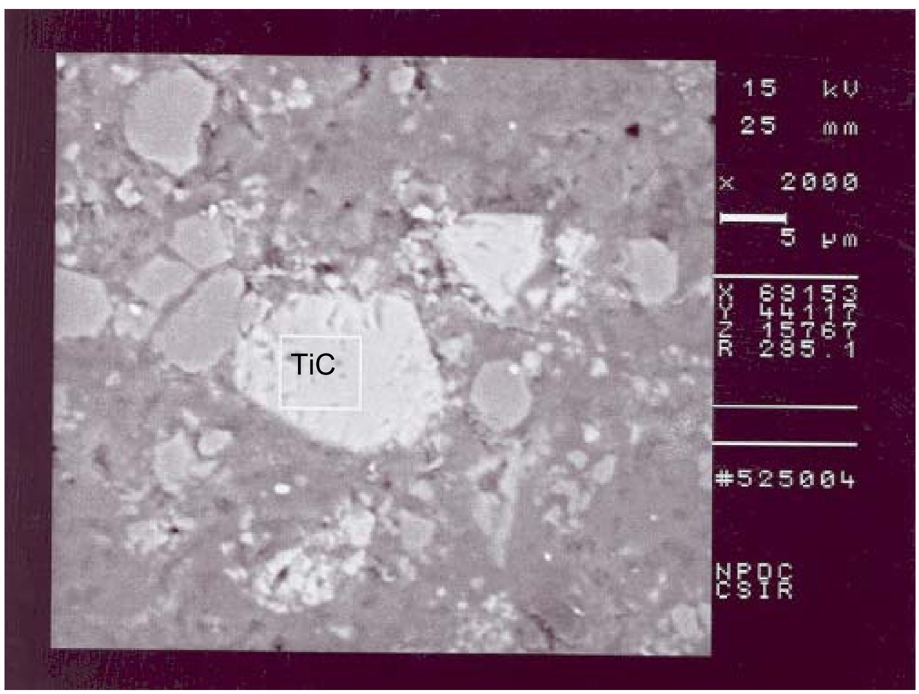

Figure 4.10: TiC particles in alloy Ind2B

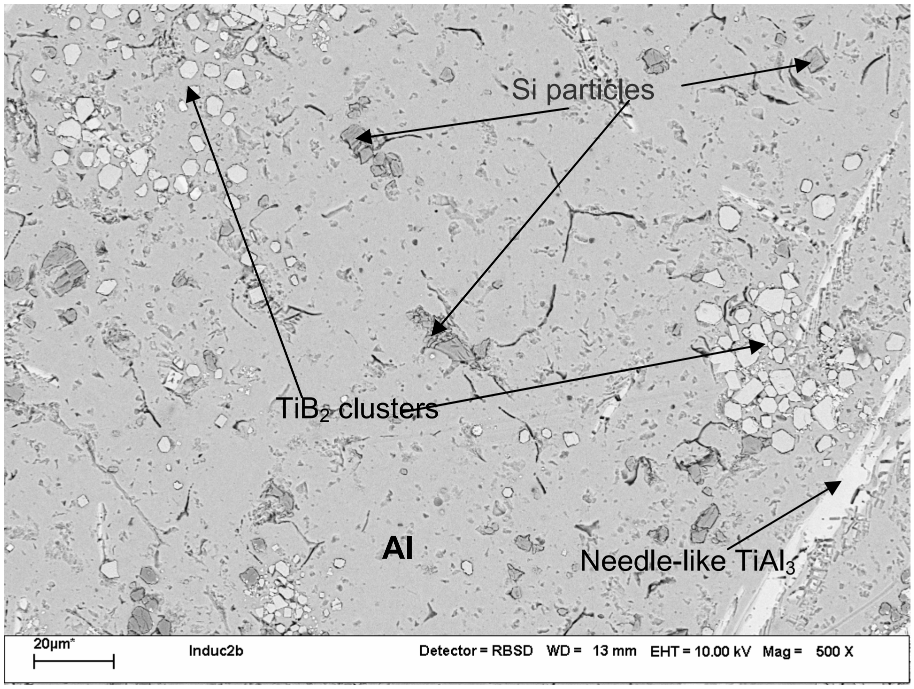

Figure 4.11: TiB_2, $TiAl_3$ and silicon particles in alloy Ind2B

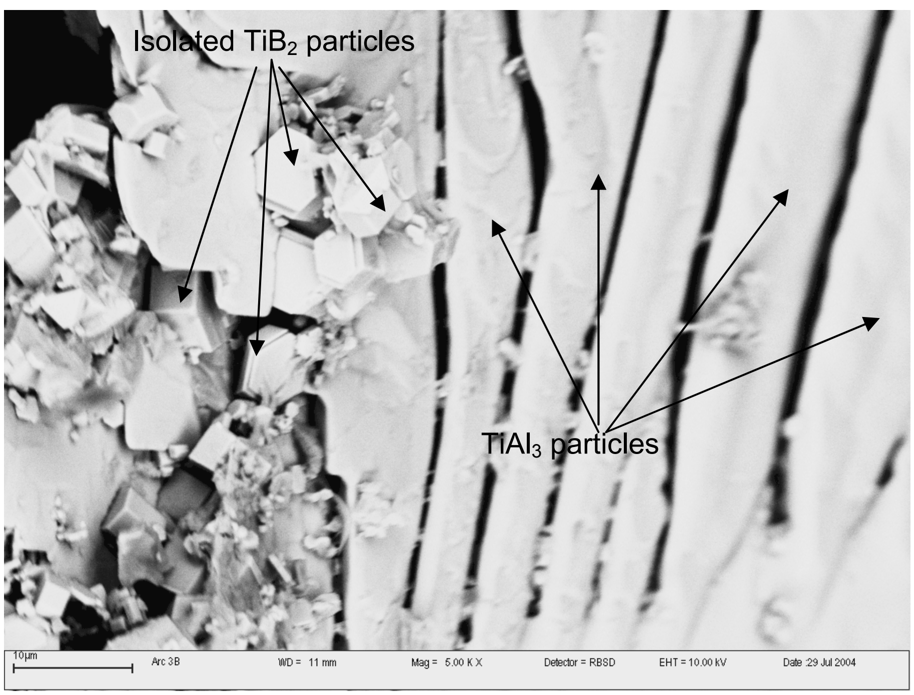

Figure 4.12: TiB_2 and $TiAl_3$ particles released after dissolution of the aluminium matrix

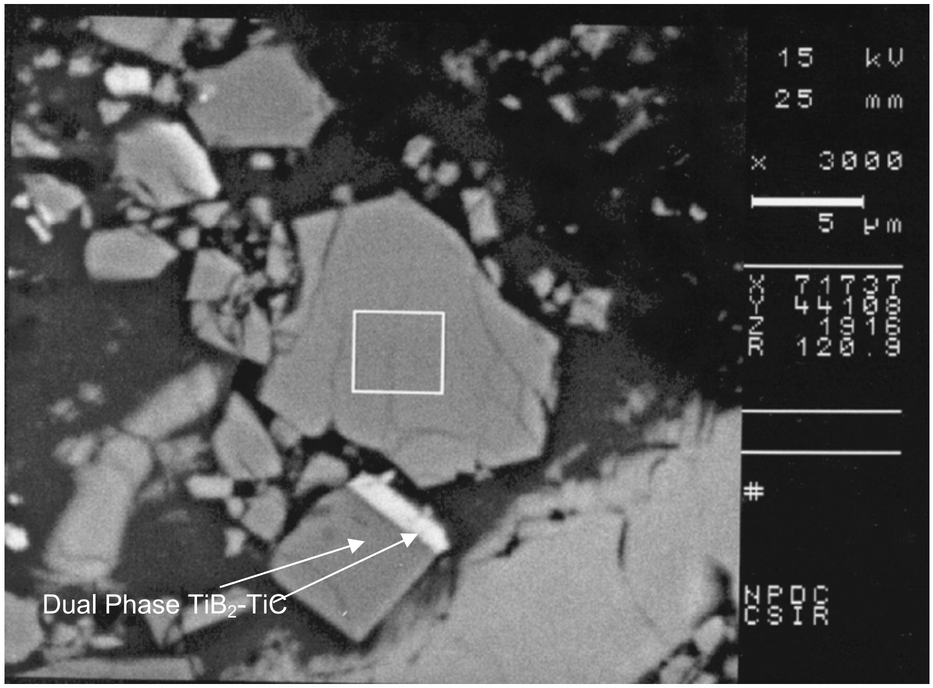

Figure 4.13 TiB_2 particle associated with TiC particles in alloy Arc2B

X-ray diffraction analyses were carried out on powder samples obtained after electrolytic dissolution of the matrix. The diffractograms showed mainly TiB_2 and $TiAl_3$ confirming these phases in the alloys. Titanium carbide peaks were not identified on the XRD pattern. This meant that, regardless of the furnace used for preparation of the alloys, $TiAl_3$ and TiB_2 were formed. A typical diffractogram obtained with alloy Arc2B is shown in Figure 4.14. Similar XRD patterns were obtained from all the samples tested.

4.3 Size of Precipitate Particles in Grain refiners

The size of $TiAl_3$ and TiB_2 particles in the grain refiners was measured. For $TiAl_3$ particles, the particle length was taken as the size of the particle. The minimum size was taken as less than 10μm and the maximum was measured. Results are presented in Table 4.3. Comparison of Tables 4.3 and 4.1 shows that the coarsest $TiAl_3$ particles occurred in grain refiners with high titanium contents. The size of TiB_2 particles ranged from 0.10 μm up to 15 μm. Statistic analyses were carried out on the size distribution of TiB_2 particles and the results are given in Table 4.4. Appendix C gives the experimental data used to draw the curves in Figure 4.15.

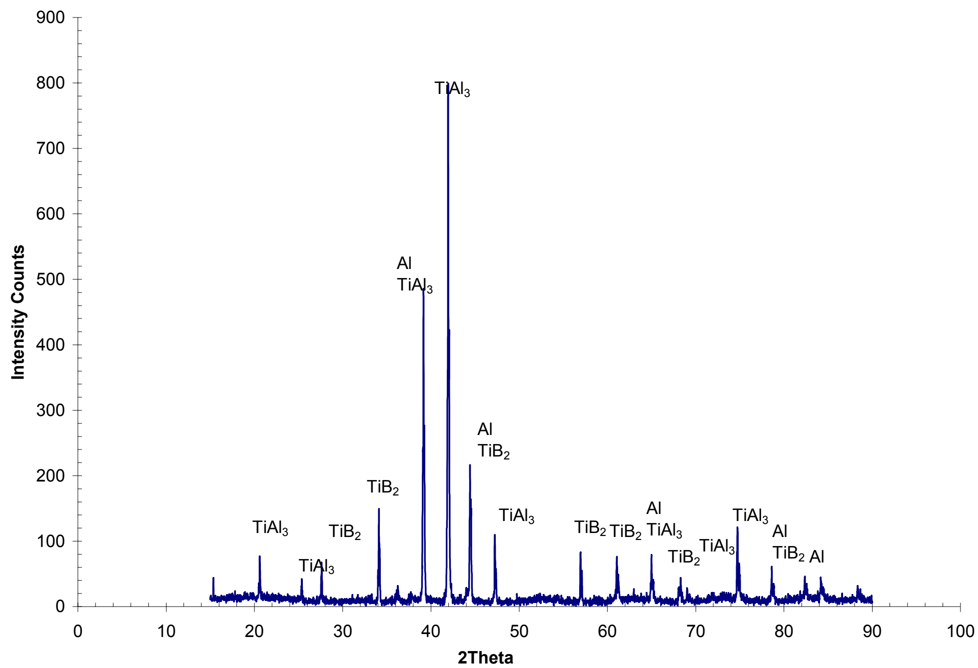

Figure 4.14: Typical XRD pattern for powder grains obtained from alloy Arc2B

Table4.3: Size limit of $TiAl_3$ particles

Grain refiners	Minimum size (μm)	Maximum size (μm)
Elec1A	<10	70
Elec1B	<10	70
Ind1A	<10	70
Ind2A	<10	70
Ind1B	<16	380
Ind2B	<10	80
Arc2B	<10	300

Table 4.4: Statistical data of TiB_2 size measurements

Samples	Elec1A	Elec1B	Ind1B	Ind2B	Ind1A	Ind2A	Arc2B
Mean Size (µm)	1.47	2.00	2.74	2.37	3.2	1.34	1.80
Median	1.20	1.74	2.13	1.77	1.86	0.92	1.14
Mode	0.30	0.31	1.21	1.25	1.56	0.65	1.65
Standard Deviation	1.10	1.55	2.17	1.85	2.77	1.36	1.76
Sample Variance	1.21	2.40	4.72	3.42	7.67	1.85	3.10
Kurtosis	2.25	0.84	4.07	2.74	1.26	28.32	4.95
Skewness	1.36	1.02	1.78	1.68	1.41	4.12	2.06
Minimum (µm)	0.10	0.14	0.25	0.18	0.57	0.09	0.12
Maximum (µm)	6.72	7.94	13.37	10.49	12.28	14.60	12.10
Sum	818.39	686.93	1305.63	970.41	304.143	506.57	1135.11
Count	557	342	476	409	95	378	632
Confidence Level (95.0%)	0.09	0.16	0.20	0.18	0.20	0.14	0.14

Curves of cumulative frequency against particle size were plotted (Figure 4.15) for different grain refiners. It is evident that the majority of TiB_2 particles in these grain refiners were smaller than 6 µm. Nevertheless the curves show significant differences between grain refiners.

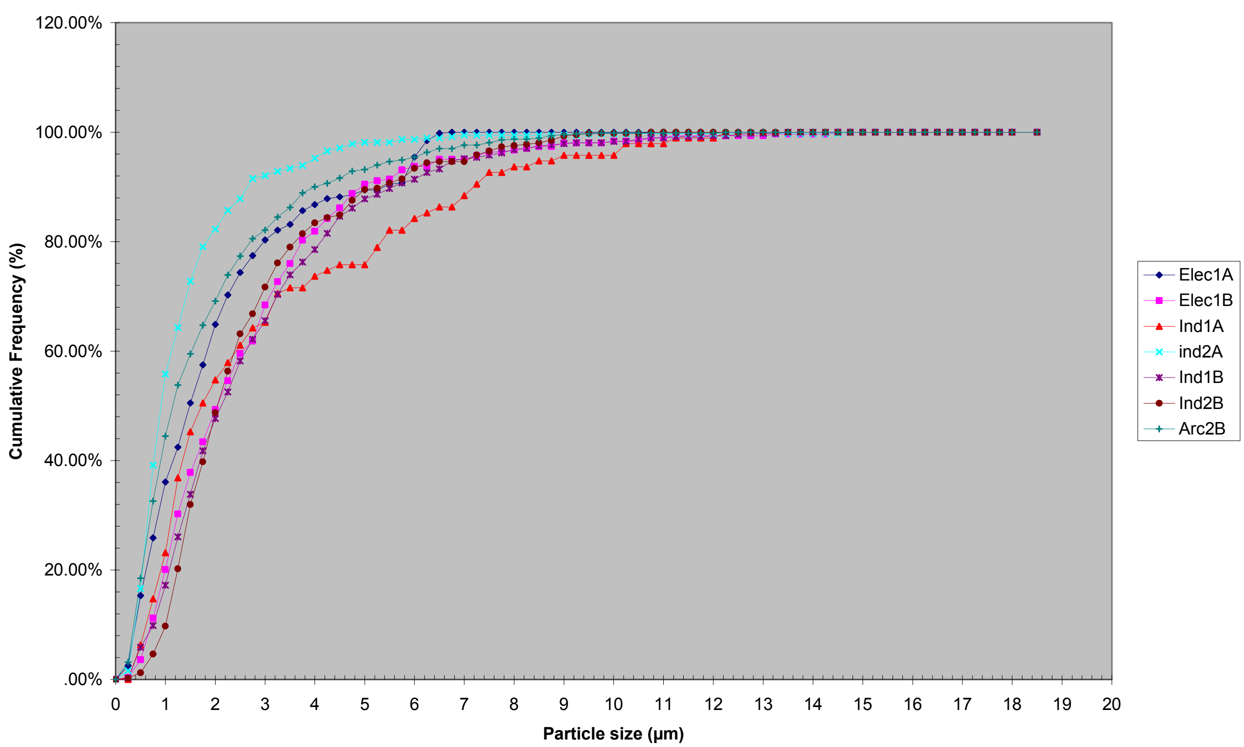

Figure 4.15: Size distribution of TiB_2 particles in different alloys

A close examination of the curves in Figure 4.15 shows that the proportion of coarse particles varies as is shown in Table 4.5. From these proportions of coarse TiB_2 particles, it becomes evident that the particle size in alloy Ind2A was close to that of commercial grain refiners, for which almost 100% of the particles are smaller than 3 μm.

Table 4.5: Relative amount of TiB_2 particles in different alloys

Alloys	Relative Amount of TiB_2 Particles (%)	
	<1μm	>3μm
Elec1A	36	20
Elec1B	20	32
Ind1A	23	26
Ind2A	56	8
Ind1B	17	34
Ind2B	10	30
Arc2B	44	20

The influence of chemical composition on the size of TiB_2 particles was also investigated. The titanium-to-boron ratio (Table 4.2) seemed to be of no consequence with respect to the size and morphology of the TiB_2 in the aluminium matrix. However, a relationship between the titanium content and the $TiAl_3$ particle size was evident. This size increased with increasing titanium content, the coarsest aluminide particles being present in alloys Arc2B (300μm) and Ind1B (380μm) which had high titanium contents.

4.4 Thermal and Mechanical Treatments

4.4.1 Microstructure after cold rolling

After cold rolling, prepared samples were examined with the optical and scanning electron microscopes. The samples were then annealed and re-examined. Particle size measurements were performed to assess the size of the boride particles after cold rolling and draw comparisons. Typical microstructures after different amount of cold deformation are shown in Figures 4.16 to 4.22. At 20% reduction no change can be seen in the orientation of $TiAl_3$ particles. They are still randomly oriented. Minor change in the orientation of $TiAl_3$ particles are observed at 40% reduction. It can be seen that the $TiAl_3$ particles show evidence of orientation at about 60% reduction. At 80% reduction $TiAl_3$ particles are broken up and aligned in the rolling direction. The microstructure of alloy Arc2B at 40% reduction is shown in Figure 4.17. Minor orientation effects due to rolling are evident. Similar effects were observed in the rest of the alloys (Elec1A, Elec1B, Ind1A, Ind2A, Ind1B and Ind2B) reduced by the same amount. Orientation effects and fragmentation of the $TiAl_3$ particles became more pronounced with increased amounts of cold rolling. Typical microstructures are shown in Figures 4.18 and 4.19 for alloys Arc2B and Elec1B respectively after 60% reduction. Similar effects were observed in other alloys at 60% reduction. As indicated earlier, at 80% reduction fragmentation and alignment of $TiAl_3$ particles were evident. Typical microstructures after 80% reduction are shown in Figure 4.20 to 4.22 for alloys Elec1B, Ind1B and Arc2B respectively.

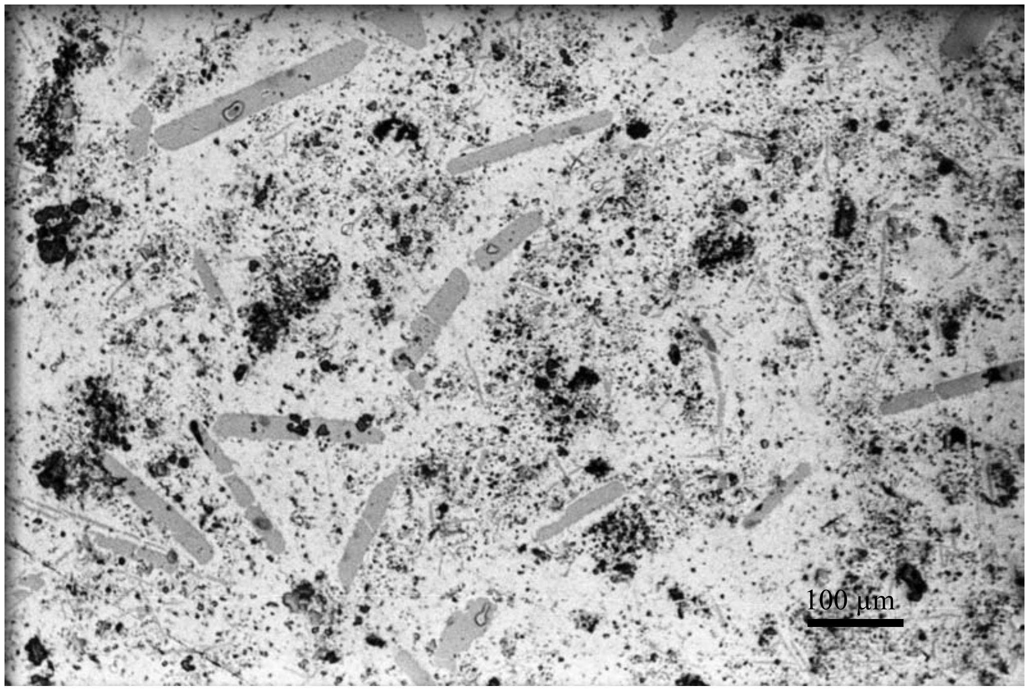

Figure 4.16: Optical micrograph of alloy Ind1B at 20 % reduction

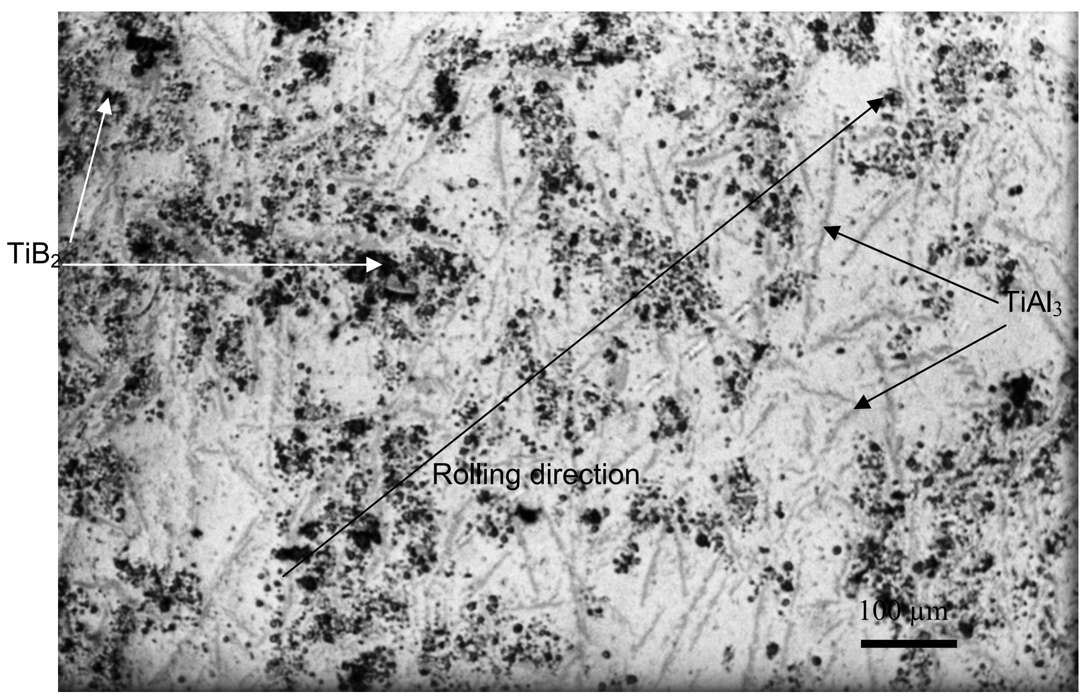

Figure 4.17: Optical micrograph of alloy Arc2B at 40 % reduction

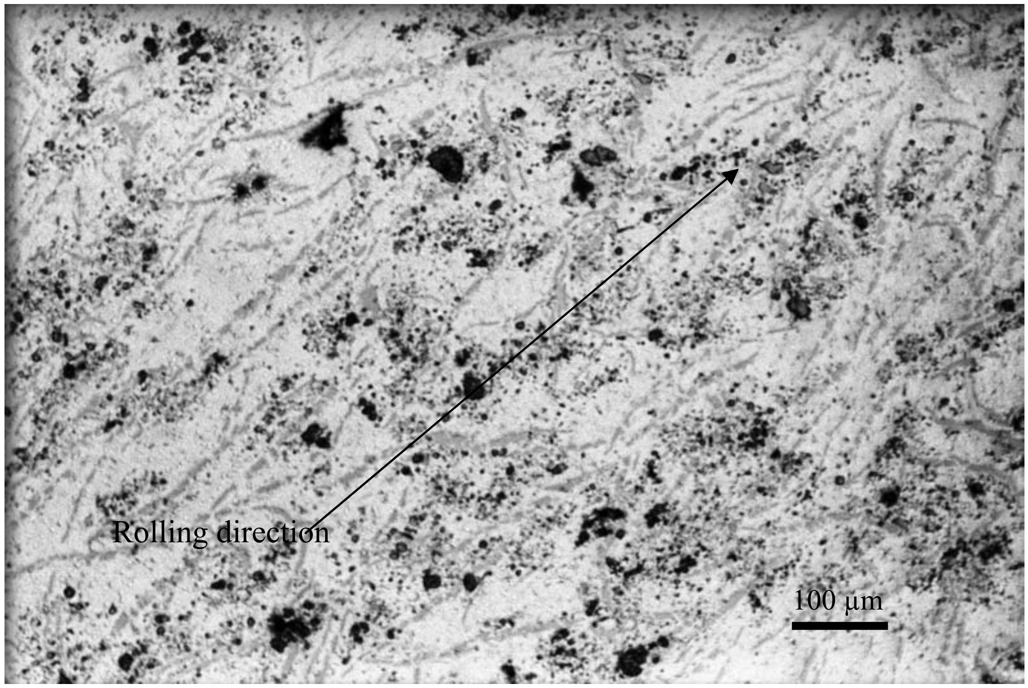

Figure 4.18: Optical micrograph of alloy Arc2B at 60 % reduction

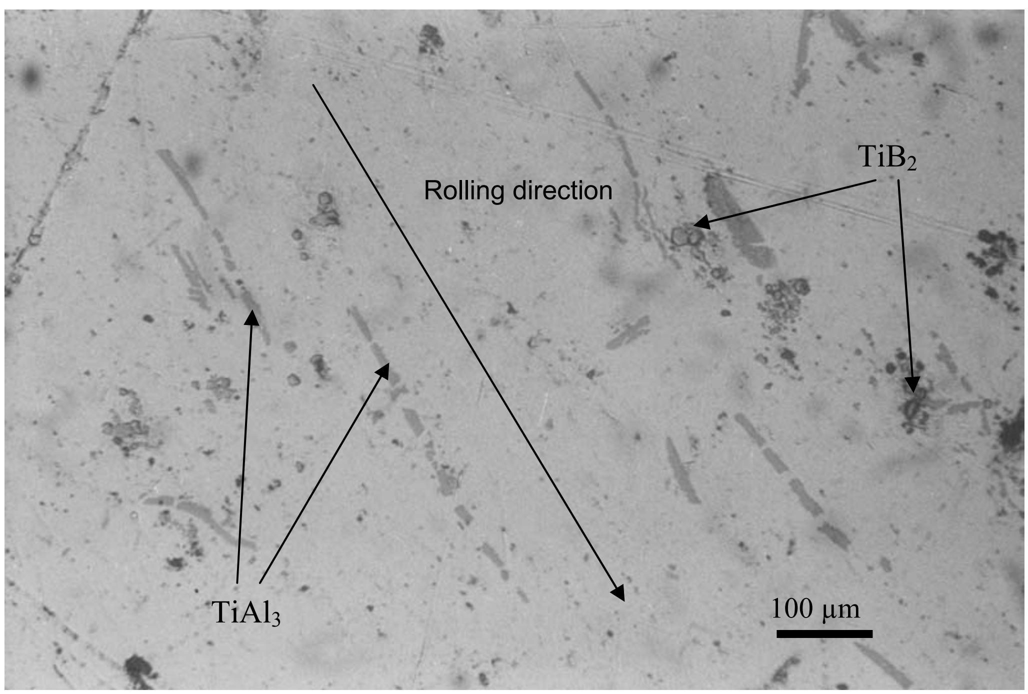

Figure 4.19: Optical micrograph of alloy Elec1B at 60 % reduction

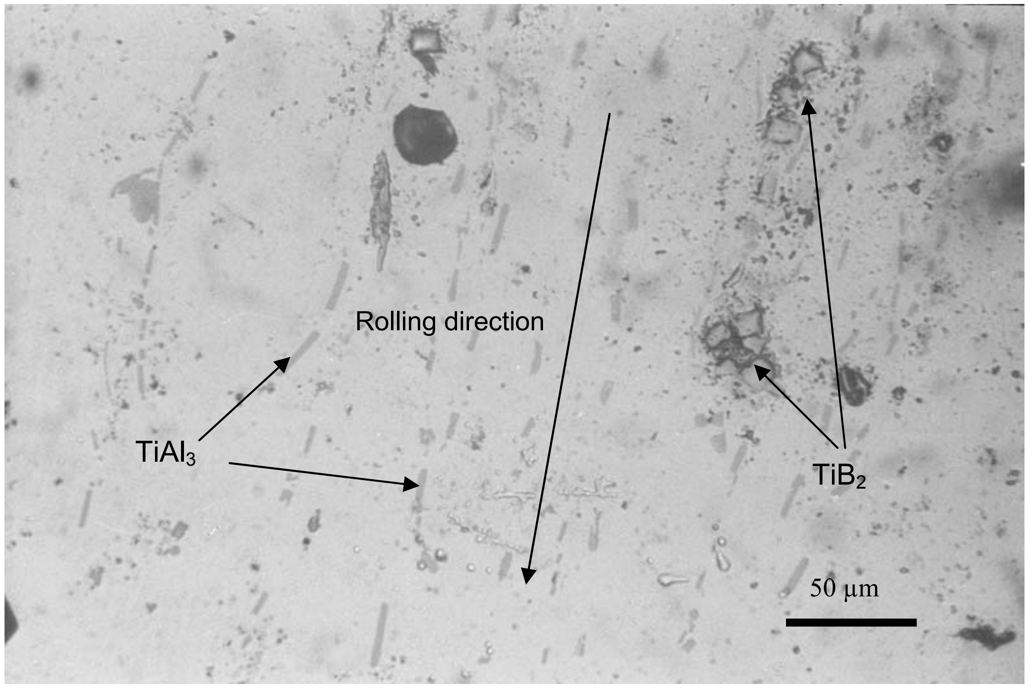

Figure 4.20: Optical micrograph of alloy Elec1B at 80 % reduction

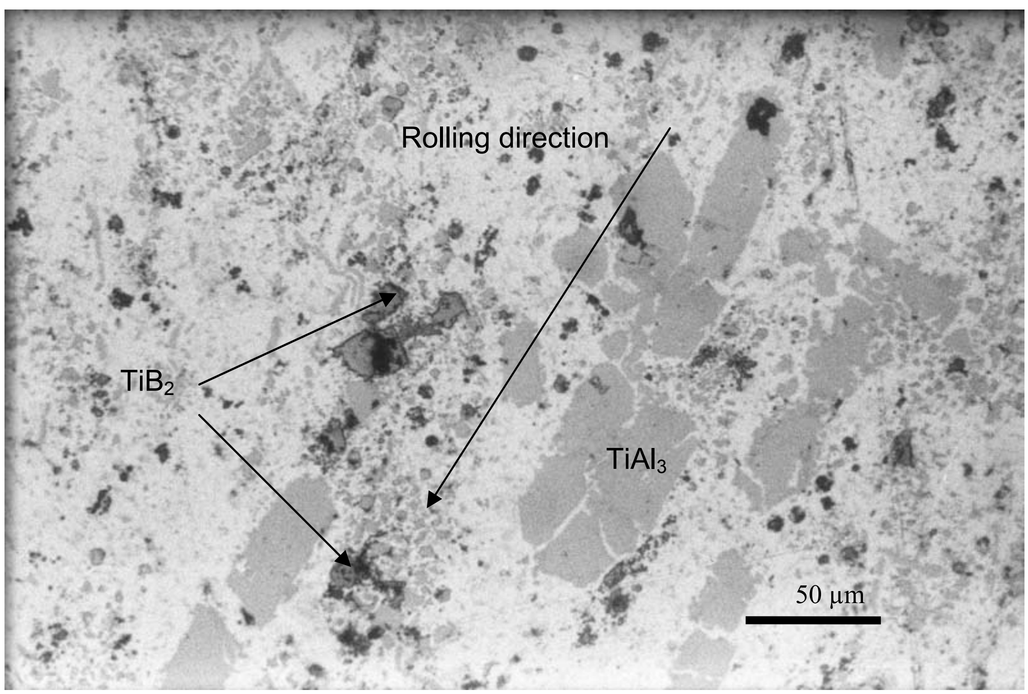

Figure 4.21: Optical micrograph of alloy Ind1B at 80% reduction

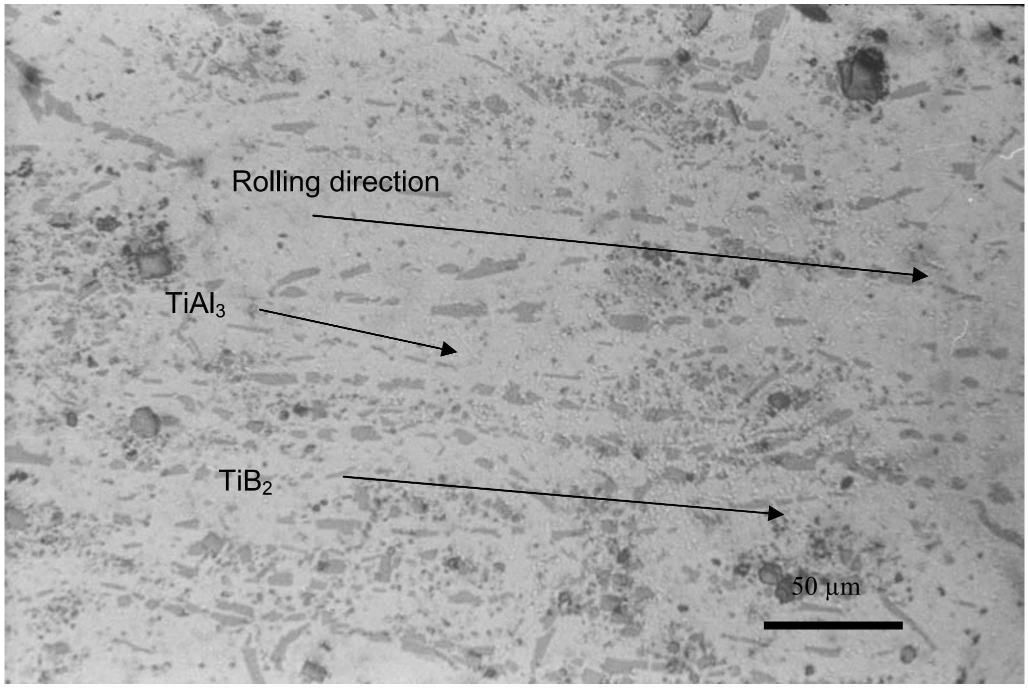

Figure 4.22: Optical micrograph of alloy Ind1B at 80% reduction

The SEM micrographs in Figures 4.23 to 4.25 show clearly the breakage of $TiAl_3$ particles. Figure 4.24 shows the parallel rows of broken $TiAl_3$ particles and cluster of TiB_2 particles in alloy Elec1B. The morphology of TiB_2 is the same as in the as-cast grain refiners. After 80% reduction, $TiAl_3$ in alloy Elec1B have lost their star-like presentation and are now showing up as dashed line oriented in the rolling direction, with most of them being elongated. As a result of high rolling reduction, the flaky titanium aluminides have been broken apart giving rise to small particles aligned in the aluminium matrix while the TiB_2 particles have kept their initial morphologies. In addition, there is a fine distribution of small blocky $TiAl_3$ particles as illustrated in Figure 4.23.

A typical microstructure of a commercial grain refiner produced by extrusion is given in Figure 4.26. This microstructure shows preferred orientation corresponding to the direction of extrusion. Blocky $TiAl_3$ particles aligned in the direction of extrusion can be seen in this micrograph but the TiB_2 particles are very small and not easily resolved.

To evaluate the change in size of titanium diboride particles, particle size measurement was performed after cold rolling. Comparison has been made between the particle sizes before and after cold rolling and results are shown in Figures 4.27 to 4.29 for alloys Ind1B, Arc2B and Ind2B. Similar curves could be drawn for others alloys.

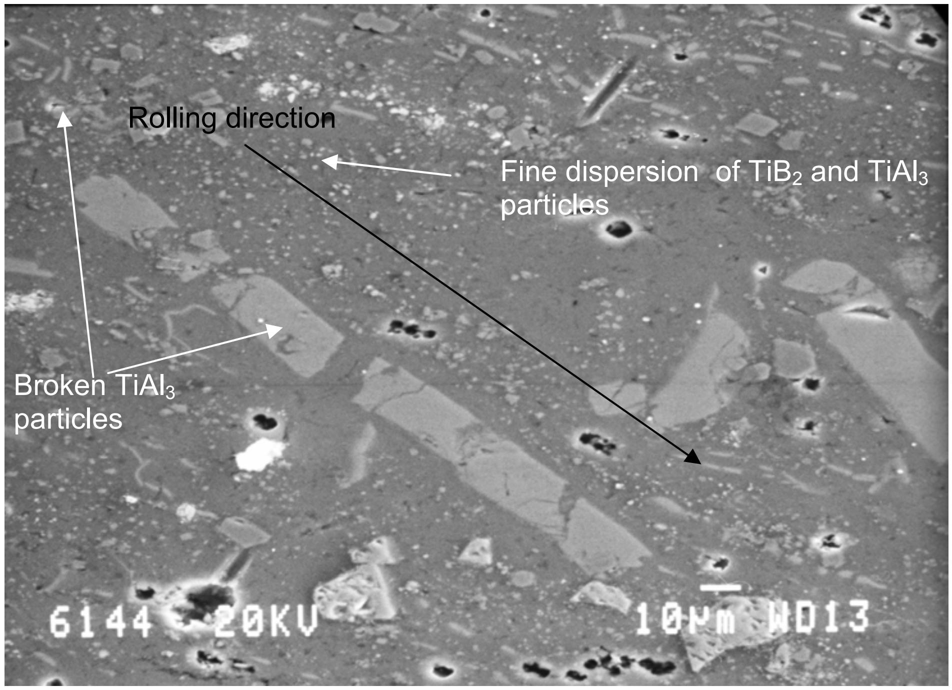

Figure 4.23: SEM micrograph of alloy Ind1B at 80% reduction

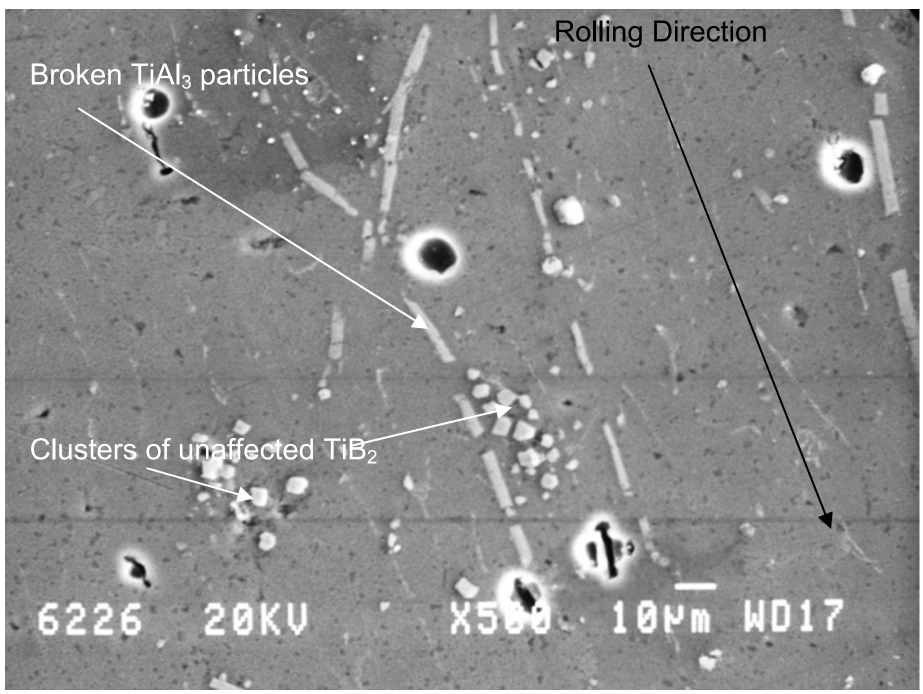

Figure 4.24: SEM micrograph of alloy Elec1B at 80% reduction

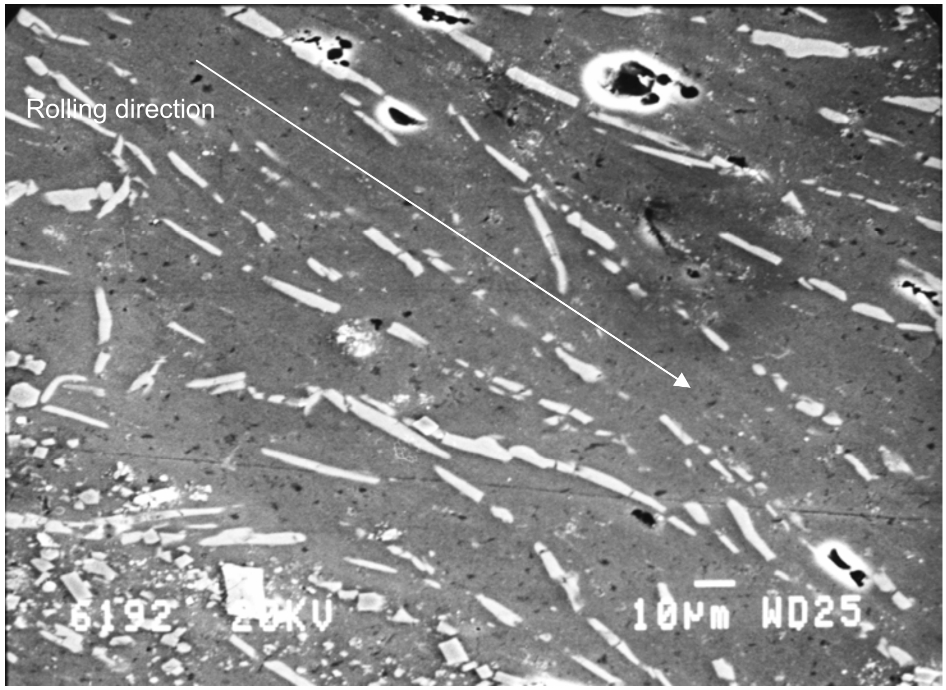

Figure 4.25: SEM micrograph of alloy Arc2B at 80% reduction

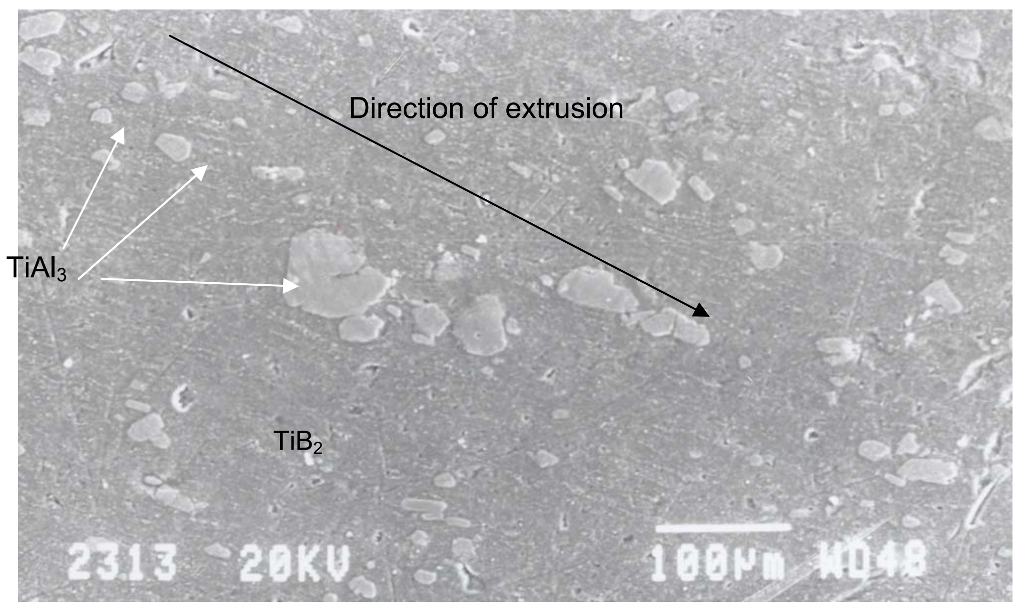

Figure 4.26: SEM micrograph of commercial Al-5Ti-1B (KBM) grain refiner

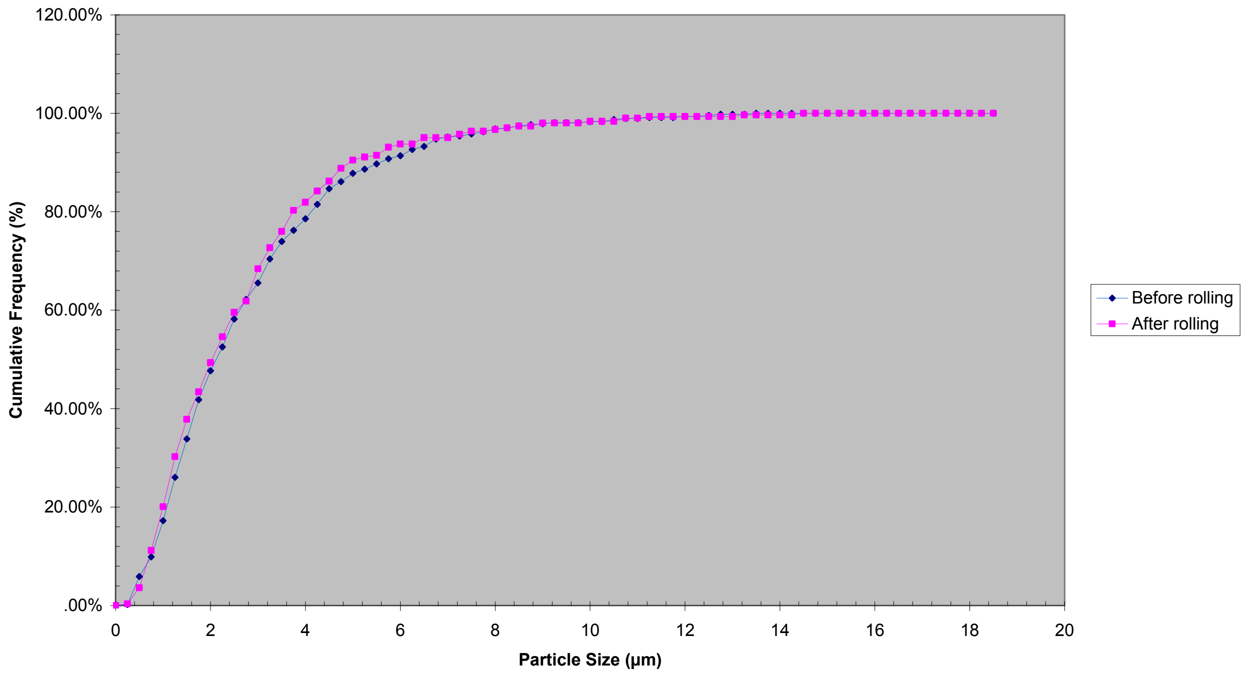

Figure 4.27: Size distribution curves of TiB2 particles before and after rolling for alloy Ind1B

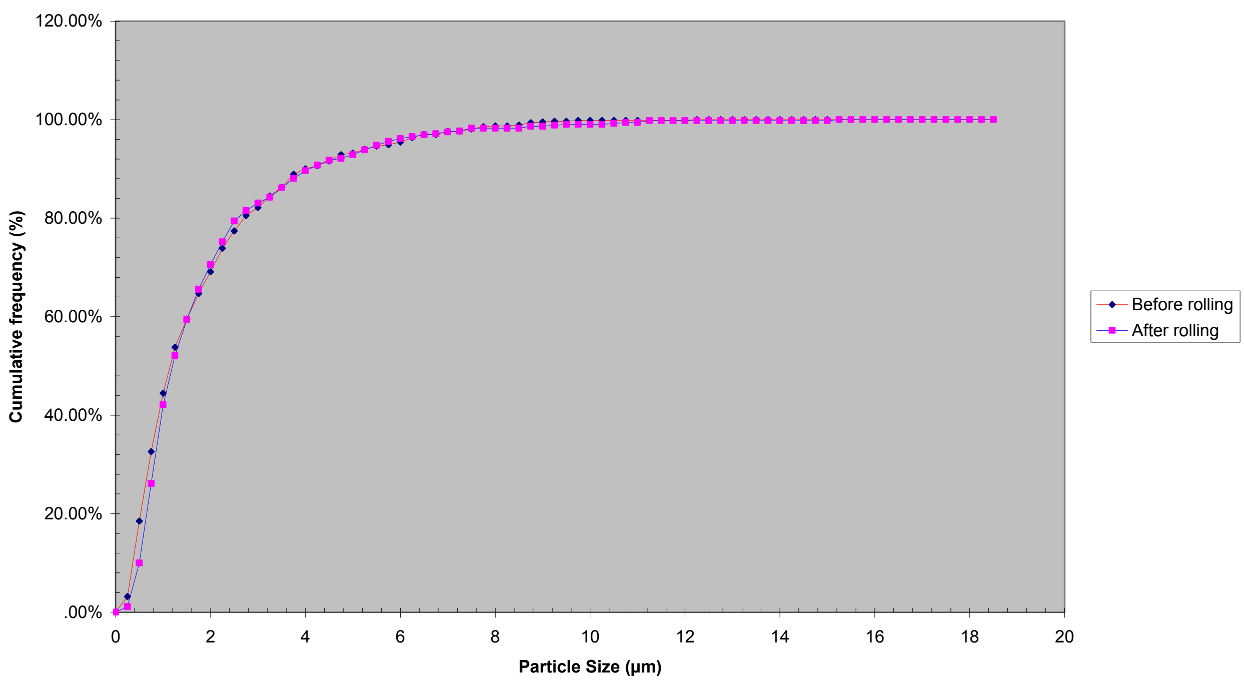

Figure 4.28: Size distribution curves of TiB2 particles before and after rolling for alloy Arc2B

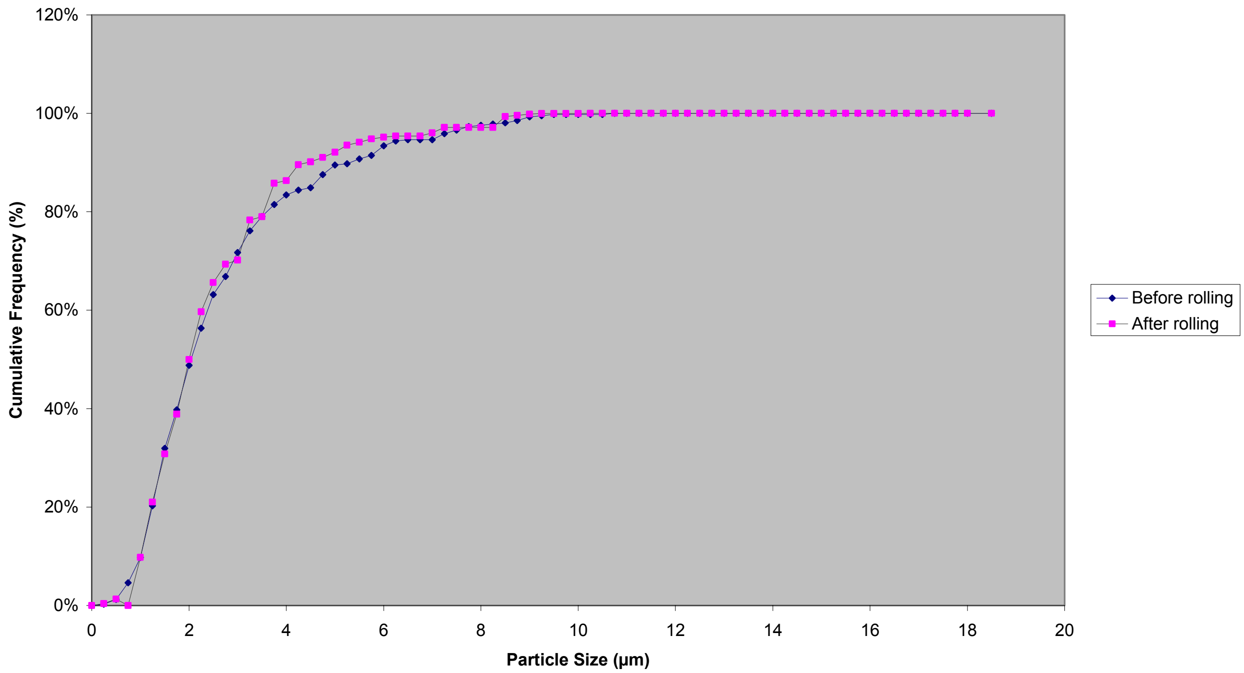

Figure 4.29: Size distribution curves of TiB2 particles before and after rolling for alloy Ind2B

From the comparatives curves, Table 4.6 could be drawn, giving the relative amount of TiB_2 particles smaller than 1µm and bigger than 3µm. Table 4.7 allowed to compare data in Tables 4.5 and 4.6.

Table 4.6: Relative amount of TiB_2 particles in alloys after cold rolling

Alloys	**Relative Amount of TiB_2 Particles (%)**	
	<1µm	**>3µm**
Ind1B	20	32
Ind2B	16	30
Arc2B	42	16

Table 4.7: Amounts of TiB_2 particles in alloys before and after cold rolling

Alloys	**Relative Amount of TiB_2 Particles (%)**			
	<1µm		**>3µm**	
	Before Rolling	After Rolling	Before Rolling	After Rolling
Ind1B	17	20	34	32
Ind2B	10	14	30	30
Arc2B	44	42	20	16

It can be seen from Table 4.7 that the amount of fine and coarse TiB_2 particles was almost unchanged before and after rolling. The rolling process did not induce any significant change in TiB_2 size in the overall distribution from particles bigger to particle smaller than 3μm.

4.4.3 Microstructure after cold rolling and annealing

After cold rolling and heat treatment, the microstructure showed the usual aluminium matrix, blocky TiB_2 particles and $TiAl_3$ particles with smooth rounded edges. The TiB_2 particles were unaffected by the heat treatment while $TiAl_3$ particles showed rounding effects. The rough edges of broken $TiAl_3$ were now smooth and rounded as can be seen from Figure 4.30. A similar microstructure was obtained with other grain refiners.

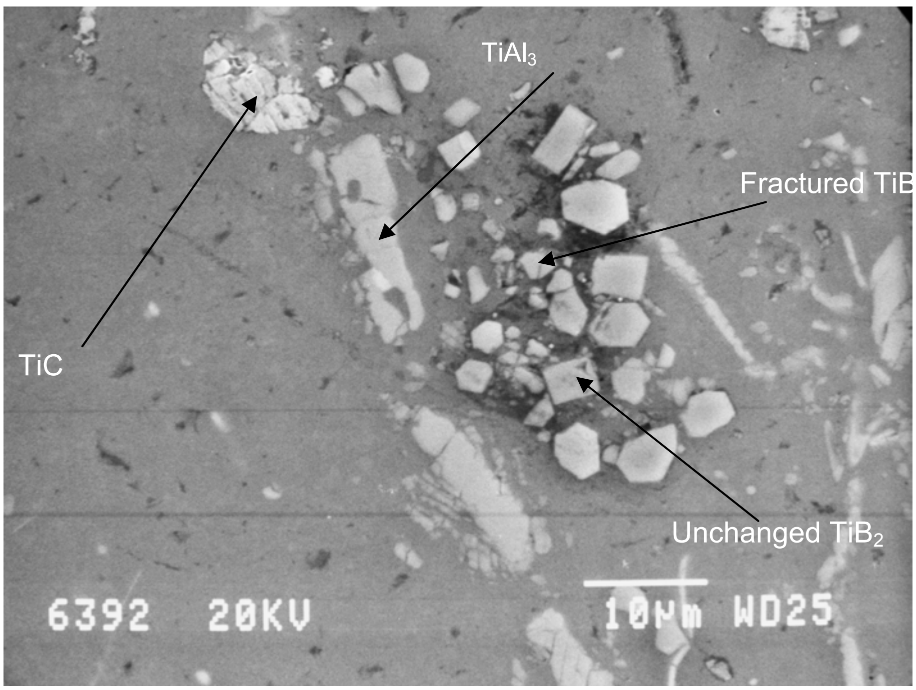

Figure 4.30: SEM micrograph showing $TiAl_3$ and TiB_2 with smooth edges in alloy Elec1B

4.5 Hardness Tests

Hardness tests were carried out on grain refiners in the as-cast condition, after cold rolling and after cold rolling and annealing. The results of hardness test are presented in Table 4.8, and illustrate the changes in hardness in the materials during the mechanical and thermal processing. From Table 4.8, it can be seen that Elec1A, Ind1A, Ind1B and Ind2B are practically of the same hardness as commercial grain refiners TiBAl and TiCAl[315] at about 36HV. Alloy Elec1B was significantly softer at 26HV while alloys Ind2A and Arc2B were significantly harder at about 46HV. The hardness of cold rolled alloys was substantially higher than that of the as cast alloys.

Annealing had a significant softening effect generally, reducing the hardness to close its original value. As expected, there was an increase in hardness after cold rolling and a loss of hardness after annealing. As a result, there was no change in the overall hardness of grain refiners after cold rolling followed by annealing.

Table 4.8: Vickers hardness of grain refiners as-cast, cold rolled by 80% and cold rolled and annealed.

SAMPLES	HARDNESS, HV5		
	AS-CAST	COLD-ROLLED	COLD-ROLLED AND ANNEALED
Elec1A	36	70	35
Elec1B	26	54	30
Ind1A	31	63	35
Ind2A	49	74	46
Ind1B	37	70	40
Ind2B	32	66	34
Arc2B	46	70	46
TiBAl	36*	-	-
TiCAl	36*	-	-

*As-cast and extruded

4.6 Grain Size Measurements

The grain size of the aluminium inoculated with as-cast, cold rolled and cold rolled and annealed grain refiners was assessed and is shown in Table 4.9. Plots of grain size against melt holding time are shown in Figure 4.31 to 4.35. It is evident that the addition of grain refiners resulted in substantial reduction in grain size in all cases compared to material cast without grain refiners and the effect of the grain refiners was probably immediate upon addition. Maximum benefit is gained for holding periods of less than 5 minutes. For holding times of over 5minutes the grain size remained constant or even increased. The target size of 220μm was not achieved with the grain refiners. The finest size achieved with Ind2A was only 236μm.

Overall there was a decrease in grain size when the cold rolled grain refiners were used to inoculate the melt. Data in Tables 4.9 and 4.10 give an indication about a relationship found between the hardness of the grain refiners (Table 4.8) and their grain refining performance. The higher the values of hardness, the smaller the grain size of inoculated aluminium. As-cast and mechanically and thermally treated grain refiners which showed low values of hardness produced a relatively big grain size in the inoculated aluminium.

Table 4.10 gives the extent of grain size reduction for each holding time. This reduction was calculated according to the following formulae:

GS Reduction % = (GS achieved with as-cast GR – GS achieved with cold rolled or annealed GR)*100/GS achieved with as-cast GR

Where GS is grain size and GR is grain refiner.

The negative values in grain size reduction correspond to poorer grain refining ability. As can be seen from Table 4.10, the targeted grain size of 220µm was not reached despite the fact that grain size reductions of up to 42% were achieved. Table 4.10 also shows that the smaller the grain size achieved with the as-cast grain refiner, the higher the probability of reaching and exceeding the acceptance level of 220µm after cold rolling of the grain refiner. In this work, only alloy Ind2A submitted to cold rolling has produced a grain size lower than 220µm after 10 minutes of holding of the melt. In the other cases, although there was an improvement in the grain refining performance, the grain size achieved with the cold rolled grain refiners was still above the acceptance level. Although annealed grain refiners gave also smaller grain sizes than as-cast ones, the finest grains were achieved when the cold rolled grain refiners were used. However, cold rolled which gave good refining performance showed onset of fading earlier than as-cast and annealed grain refiners, leading in some case to coarser grains at 30 minutes of holding. This explains the negative values of grain size reduction obtained at 20 and 30 minutes of holding when the cold rolled grain refiners were used in the inoculation process (Table 4.10).

Figure 4.35 is an illustration of grain size achieved when commercial grain refiner Al-5%Ti-1%B was used in the inoculation process. From this figure, the grain size achieved is below 220µm after only 2 minutes of holding of the melt with no fading after 30 minutes.

Table 4.9: Grain size of aluminium as a function of grain refiner and holding time

Grain refiner/holding time (minutes)		**Grain size of aluminium inoculated with experimental grain refiners (µm)**		
		Alloy with as cast grain refiner	**Alloy with cold rolled grain refiner**	**Alloy with cold rolled and annealed grain refiner**
Elec1B	0	831.33	804.02	784.31
	2	465.95	261.01	398.01
	5	414.18	243.16	343.35
	10	369.19	261.01	344.83
	20	332.05	363.64	303.03
	30	399.85	403.02	354.77
In2A	0	831.33	846.56	780.49
	2	318.33	261.44	339.70
	5	327.35	225.99	334.73
	10	289.61	210.53	335.43
	20	236.3	244.65	338.27
	30	322.36	227.92	320.00
Ind1B	0	837.36	780.49	837.70
	2	479.48	316.21	414.51
	5	339.87	341.88	435.97
	10	344.94	326.53	410.26
	20	376.4	363.64	391.20
	30	337.88	353.20	398.01
Ind2B	0	786.09	765.55	754.72
	2	418.68	347.83	313.73
	5	275.13	273.04	264.46
	10	347.01	295.75	321.93
	20	333.98	407.12	315.58
	30	325.51	331.95	353.98
Arc2B	0	810.27	803.47	756.86
	2	385.36	287.75	401.01
	5	301.64	265.32	357.94
	10	326.26	323.27	390.24
	20	330.32	336.15	354.13
	30	346.52	359.03	363.28

Table 4.10: Grain size reduction as a function of grain refiner and holding time

Grain refiner/holding time (minutes)		Reduction in grain size, %	
		After cold rolling	After cold rolling and annealing
Elec1B	0	3.29	5.66
	2	43.98	14.58
	5	41.29	17.10
	10	29.30	6.60
	20	-9.51	8.74
	30	-0.79	11.27
Ind2A	0	-1.83	6.12
	2	17.87	-6.71
	5	30.96	-2.25
	10	27.31	-15.82
	20	-3.53	-43.15
	30	29.30	0.73
Ind1B	0	6.79	-0.04
	2	34.05	13.55
	5	-0.59	-28.27
	10	5.34	-18.94
	20	3.39	-3.93
	30	-4.53	-17.80
Ind2B	0	2.61	3.99
	2	16.92	25.07
	5	0.76	3.88
	10	14.77	7.23
	20	-21.90	5.51
	30	-1.98	-8.75
Arc2B	0	0.84	6.85
	2	25.33	-4.06
	5	12.04	-18.66
	10	0.92	-19.61
	20	-1.76	-7.21
	30	-3.61	-4.84

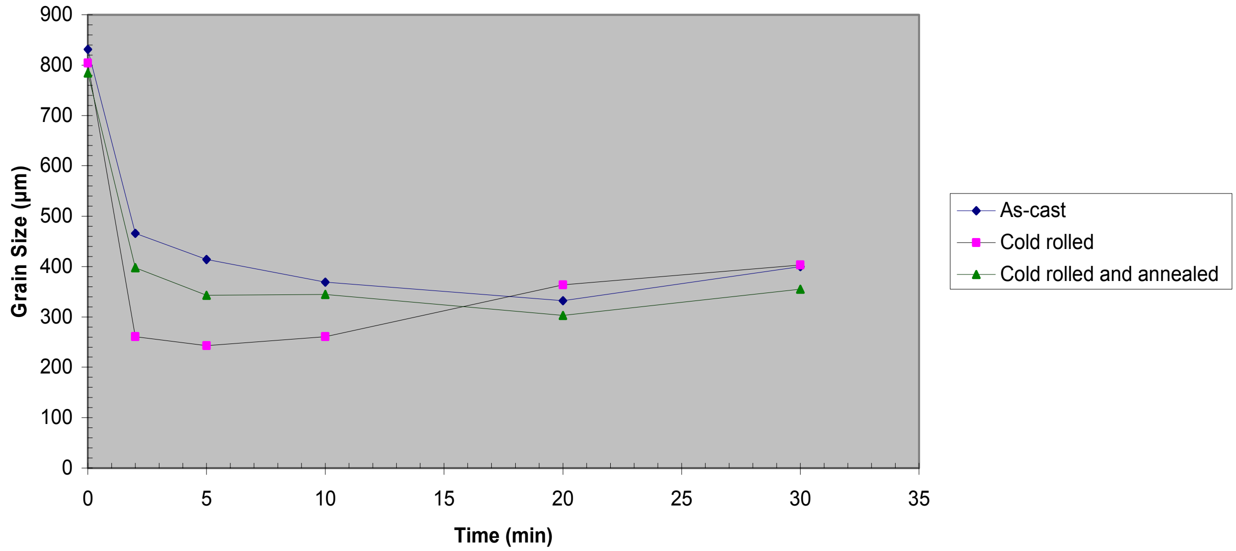

Figure 4.31: Plot of grain size against holding time for grain refiner Elec1B

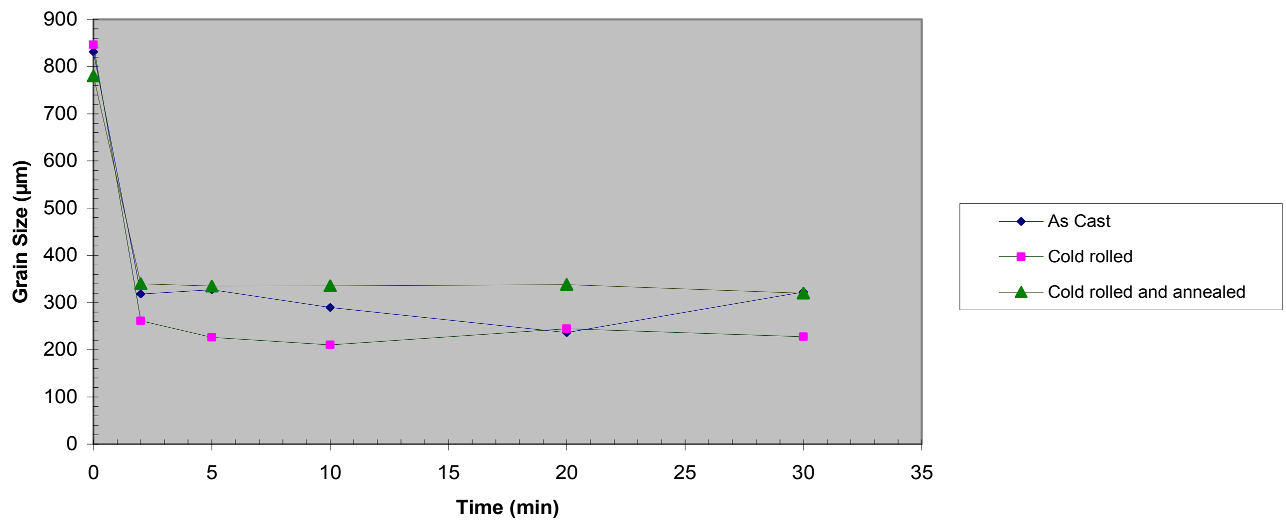

Figure 4.32: Plot of grain size against holding time for grain refiner Ind2A

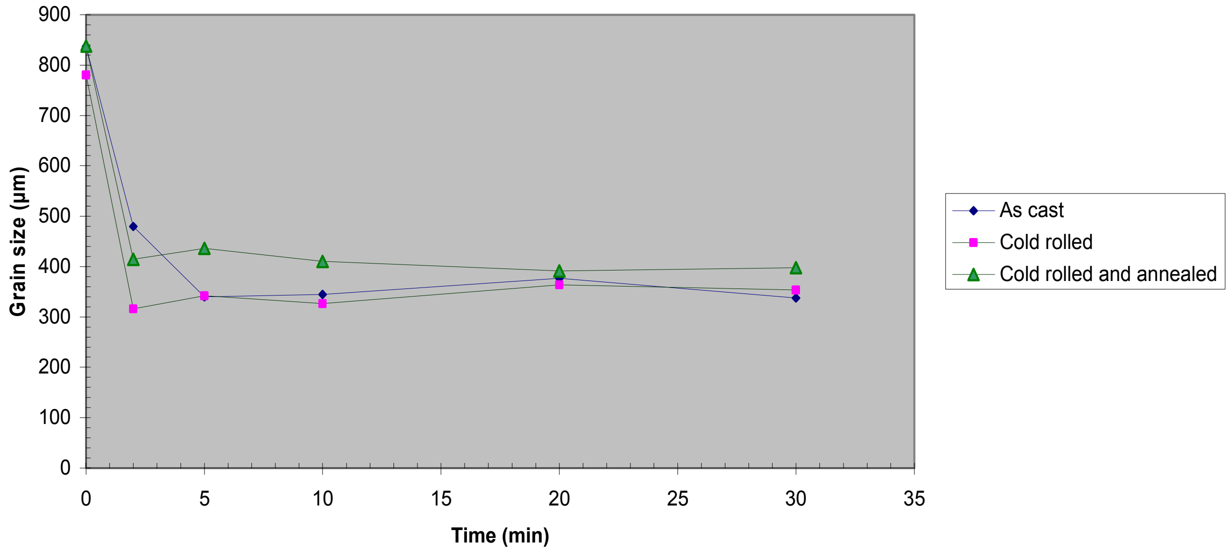

Figure 4.33: Plot of grain size against holding time for grain refiner Ind1B

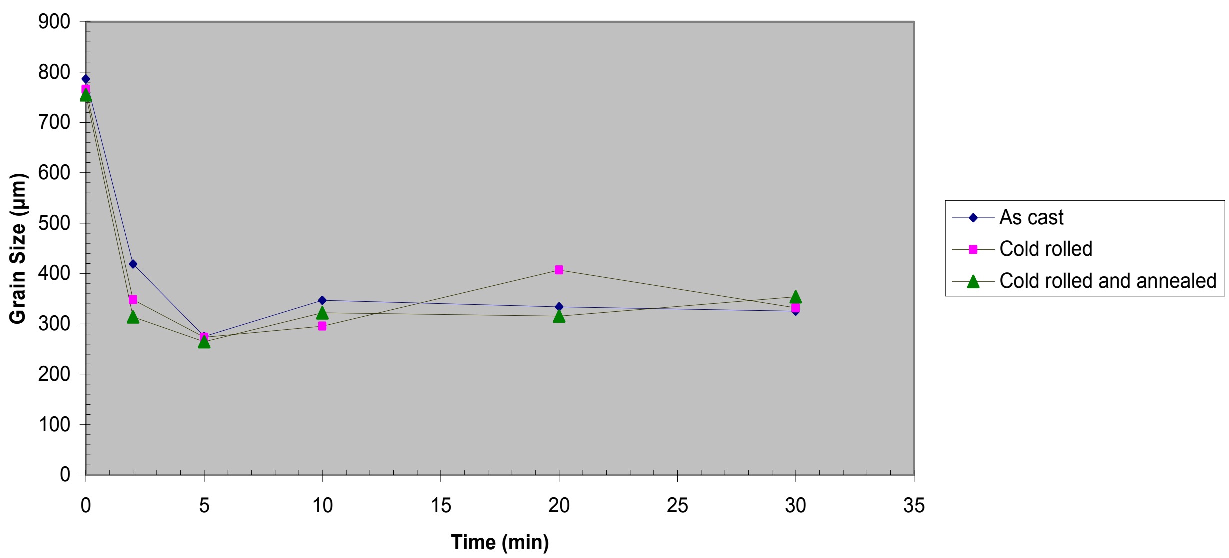

Figure 4.34: Plot of grain size against holding time for grain refiner Ind2B

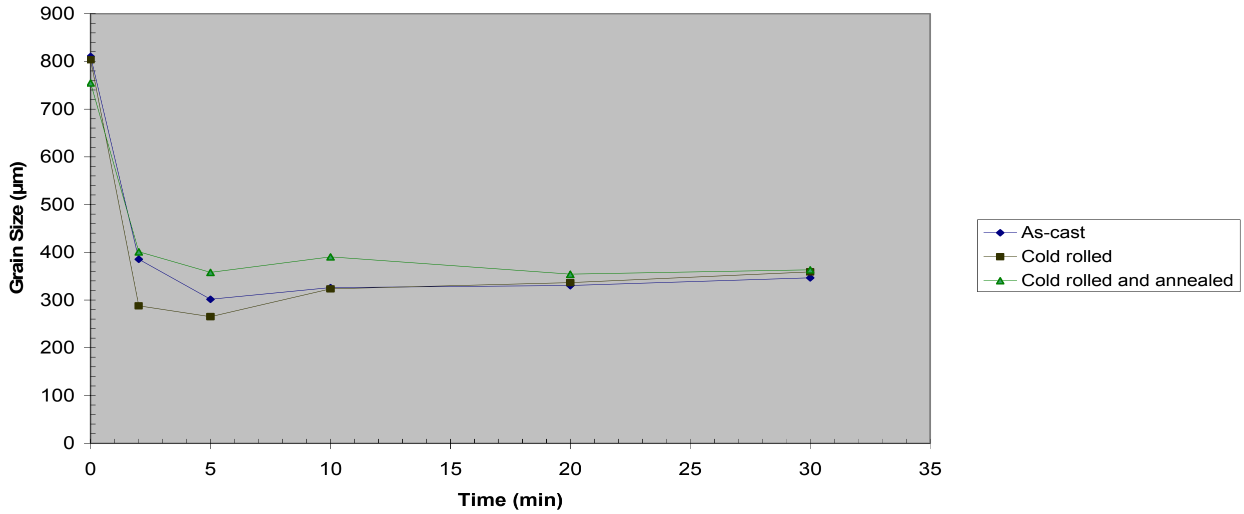

Figure 4.35: Plot of grain size against holding time for grain refiner Arc2B

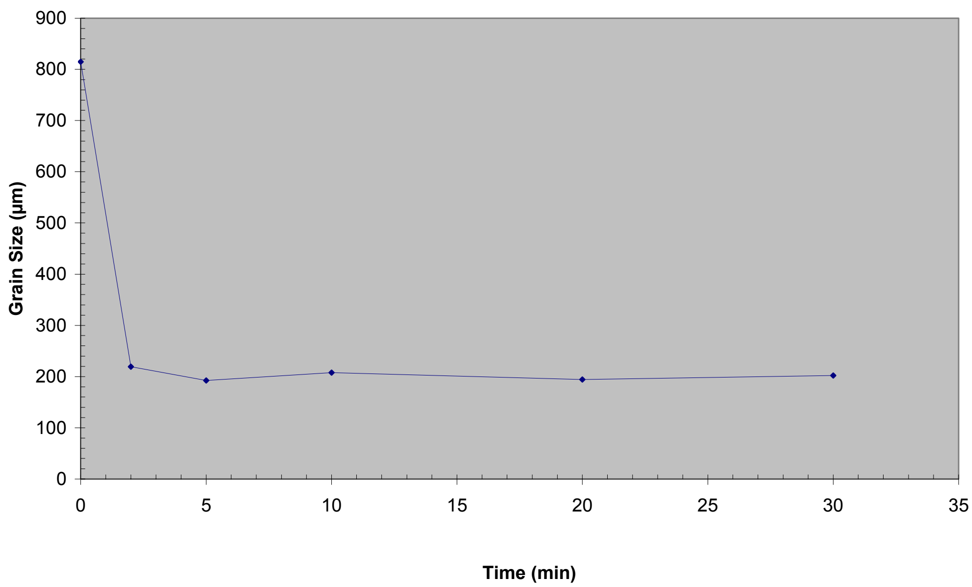

Figure 4.36: Evolution of grain size with the holding time for commercial grain refine (Al-5%Ti-1%B KBM)

Figures 4.37 and 4.38 are optical micrographs of grain sizes achieved by using experimental grain refiners and commercial grain refiners respectively. Visual inspection of these two micrographs gives an indication of the performance of the experimental and commercial grain refiners. It is evident that the experimental grain refiner was not as efficient as the commercial material. In addition, in Figure 4.37 there is a mixture of fine and coarse grains with the number of coarse grains being dominant.

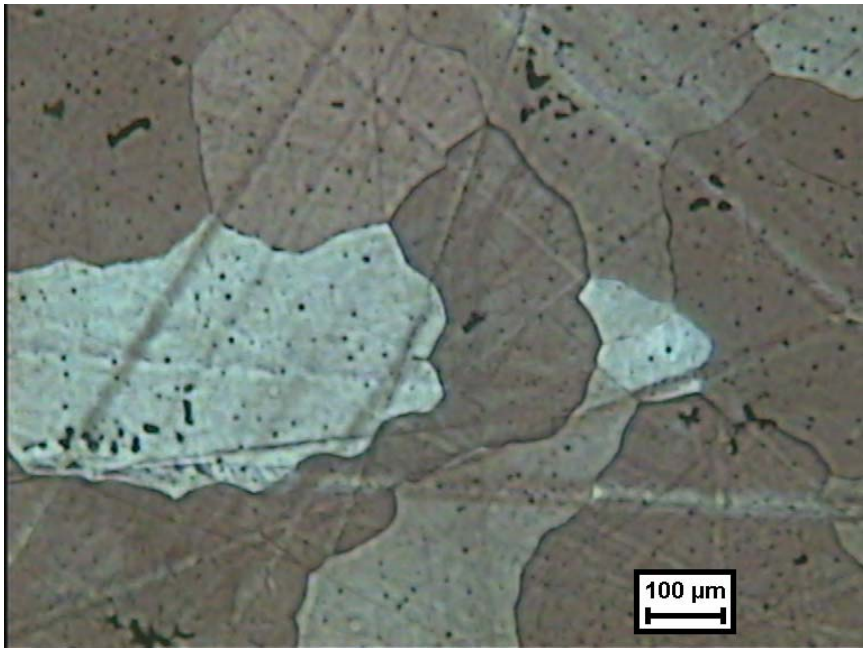

Figure 4.37: grain size achieved using an experimental grain refiner (Ind1B)

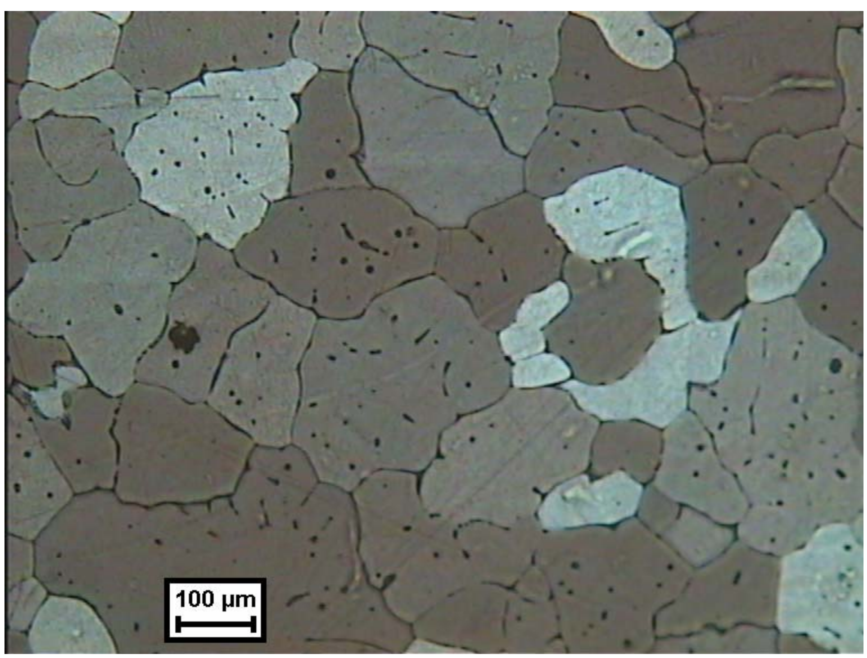

Figure 4.38: Grain size achieved using a commercial grain refiner

This observation shows that in aluminium inoculated with experimental grain refiners, grain growth was favoured at the expense of nucleation. In Figure 4.38, the sizes of grain are close, indicating simultaneous nucleation in a large number of places

4.7 Influence of Ti:B Ratio and Silicon Content on Grain Size

Table 4.11 gives the grain size of inoculated aluminium as a function of titanium-to boron ratio. This table shows that the ultimate grain size decreased with increasing Ti/B ratio and decreasing Ti and B content.

Table 4.11: Grain size as a function of titanium-to-boron ratio at the optimum contact time

As-cast sample	Ti (%)	B (%)	Ti:B	Grain Size (μm)	Time (min)
Elec1A	2.40	0.57	4.20	344.5	10
Elec1B	1.91	031	6.20	332.1	20
Ind1B	6.40	1.04	6.20	339.9	30
Ind2B	3.41	0.49	7.00	275.1	30
Ind1A	2.64	0.43	6.10	325.0	5
Ind2A	3.13	0.41	7.60	236.3	20
Arc2B	6.98	1.01	6.90	301.6	5

Table 4.12 gives the silicon content in the melt calculated from the data in Table 4.1 and the weight of the grain refiner added to 5kg of melt. From the last column in Table 4.12, the highest silicon content was found when Ind1A was added to the melt for grain refinement. For this particular case the silicon content was 0.2wt%. In the other cases, the silicon content was below 0.2wt%.

Table 4.12: Silicon content in the melt after addition of grain refiners

Samples	Weight of GR in the melt (kg)	Si content in the GR (%)	Silicon weight in the GR (kg)	Silicon weight in the CP Al (kg)	Total Si weight in the melt	Si content in the melt (%)
Elec1A	0.02	0.15	0.003	0.002	0.005	0.1
Elec1B	0.025	0.16	0.004	0.002	0.006	0.12
Ind1B	0.008	0.21	0.002	0.002	0.004	0.08
Ind2B	0.015	0.24	0.004	0.002	0.006	0.12
Ind1A	0.019	0.40	0.008	0.002	0.01	0.2
Ind2A	0.016	0.42	0.007	0.002	0.009	0.18
Arc2B	0.007	0.25	0.001	0.002	0.003	0.06
KBM	0.01	0.11	0.002	0.002	0.004	0.08

Where GR : Grain Refiner, CP al : Commercial Parity Aluminium (Table 3.3)

4.8 Comparison of the salt route and the aluminothermic reduction

Table 4.13 gives a comparison of the manufacturing route used in this work and the salt route used for commercial grain refiners. This table highlights the factors which influence the grain refining performance.

Table 4.13: Comparison of salt route and aluminothermic reduction

Factors	**Manufacture methods**	
	Salt route	**Aluminothermic reduction**
Feed materials	CP aluminium, K_2TiF_6 and KBF_4	CP aluminium, TiO_2 and B_2O_3
Reaction temperature	700-750ºC	> 800ºC
Manufacture technique	Continuous extrusion process	2 steps
Microstructure	Aluminum matrix, TiB_2 and $TiAl_3$ particles	Aluminum matrix, TiB_2 , Si , TiC and $TiAl_3$ particles
Nucleant size distribution	Narrow	Wide
Refining performance	High	Low
Grain refiner shape	Rod	Cylinder
Inoculation technique	Continuously at the launder	Manually